Solid State Sciences 105 (2020) 106209

Contents lists available at ScienceDirect

Solid State Sciences

journal homepage: http://www.elsevier.com/locate/ssscie

A study of structural, electronic, elastic, phonon properties, and transition mechanism of wurtzite CdTe under high pressure

Çağatay Yamçiçier [a], Cihan Kürkçü [b,*], Ziya Merdan [c]

[a] Institute of Science, Gazi University, 06500, Ankara, Turkey
[b] Department of Electronics and Automation, Kırşehir Ahi Evran University, 40100, Kırşehir, Turkey
[c] Department of Physics, Faculty of Arts and Sciences, Gazi University, 06500, Ankara, Turkey

ARTICLE INFO

Keywords:
Phase transition
Transition Path
Electronic structure
Elastic constants
Phonon

ABSTRACT

Ab initio computational methods based on density functional theory to study the structural, electronic, elastic and phonon properties of Cadmium Telluride (CdTe) were applied. SIESTA method was used for calculations with the generalized gradient approximation (GGA) for the exchange-correlation functional and norm-conserving Troullier-Martins pseudopotentials. Our calculations are carried out to investigate the high-pressure behavior of the hexagonal wurtzite structured CdTe corresponding to the space group of $P6_3mc$. When increased hydrostatic pressure was applied on this structure of CdTe, phase transformation was obtained to a cubic structure with space group $Fm\bar{3}m$ at 10 GPa. During this phase transformation, the transition path was predicted as follows: $P6_3mc \rightarrow P2_1 \rightarrow Cmc2_1 \rightarrow P2_1 \rightarrow P2_1/m \rightarrow Pmn2_1 \rightarrow Pmmn \rightarrow Fm\bar{3} \rightarrow Fm\bar{3}m$. As the pressure continued to increase, phase transformation to an orthorhombic structure with space group Cmmm at 140 GPa occurred. During this transformation, the transition path was predicted as follows. $Fm\bar{3}m \rightarrow R\bar{3}m \rightarrow P\bar{1} \rightarrow P4/mmm \rightarrow Cmmm$. As a result of the literature studies, the transition paths obtained in the study were estimated for the first time. In addition, the electronic properties of CdTe such as band structure and density of states for the obtained high-pressure phases were examined. Although the wurtzite structure of CdTe has a semiconductor character, the other obtained cubic and orthorhombic structures have a metallic character. In addition, in order to determine whether all phases of CdTe are mechanically and dynamically stable, we also examined the elastic and phonon properties respectively. As a result, the wurtzite and cubic structures of CdTe were determined to be both mechanically and dynamically stable, whereas the orthorhombic structure was unstable.

1. Introduction

In recent years, studies on the structure of Cadmium chalcogenides (CdX, X = S, Se, Te) under high pressure have been attracted much attention because of their technological importance as well as scientifically having wide and direct band gaps [1]. Cadmium telluride (CdTe) is one of these chalcogenides has been the subject of many studies due to its practical and widespread use in optoelectronic applications [2,3]. As in many II-VI semiconductors, cadmium chalcogenides also exist in both zinc-blend (B3) with space group $F\bar{4}3m$ and wurtzite (B4) with space group $P6_3mc$ structures [1,4,5]. Under high pressure, these B3 and B4 type chalcogenides are generally known to transform to the B1 type structure.

Mei and Lemos performed photoluminescence measurements on CdTe under hydrostatic pressure up the phase transition. They achieved phase transition at 3.9 GPa [1]. Wei and Zhang studied the cadmium chalcogenes in both the zinc blende and the wurtzite type. They found that at low temperatures the structure of the zinc blende CdTe was more stable than wurtzite type structure. However, they said that wurtzite structure could be more stable with coherent substrate strain. Furthermore, they suggested that wurtzite CdTe had a wide bandgap than the zinc blende structure. The phase transition sequence observed in the literature in general is from zinc blende structure to cinnabar structure (at 2.0–3.5 GPa), from this structure to B1 structure (at 3.5–3.8 GPa) and finally from B1 to Cmcm structure (at 10 GPa) [6]. Besides, McMahon et al. [7] explained that under increased pressure up to 5 GPa, CdTe in the zinc blende structure transformed into a trigonal cinnabar type structure with the space group $P3_121$ at 3.53 GPa. When they continued

* Corresponding author.
E-mail address: ckurkcu@ahievran.edu.tr (C. Kürkçü).

https://doi.org/10.1016/j.solidstatesciences.2020.106209
Received 17 January 2020; Received in revised form 24 February 2020; Accepted 9 April 2020
Available online 16 April 2020

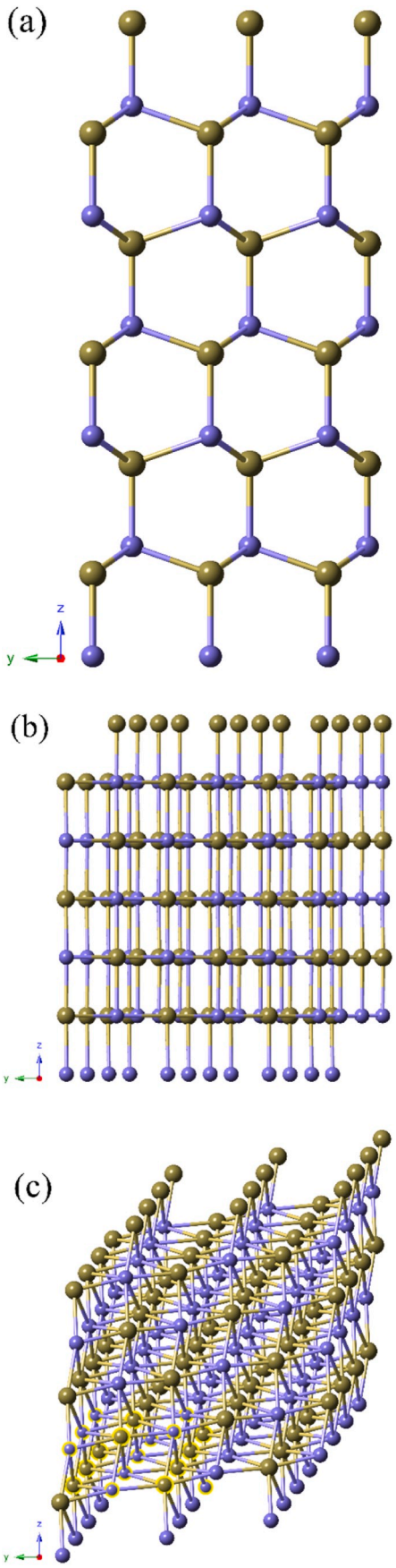

Fig. 1. Crystal structures of CdTe:P6$_3$mc at 0 GPa (top), Fm$\bar{3}$m at 10 GPa (middle) and Cmmm at 140 GPa (bottom).

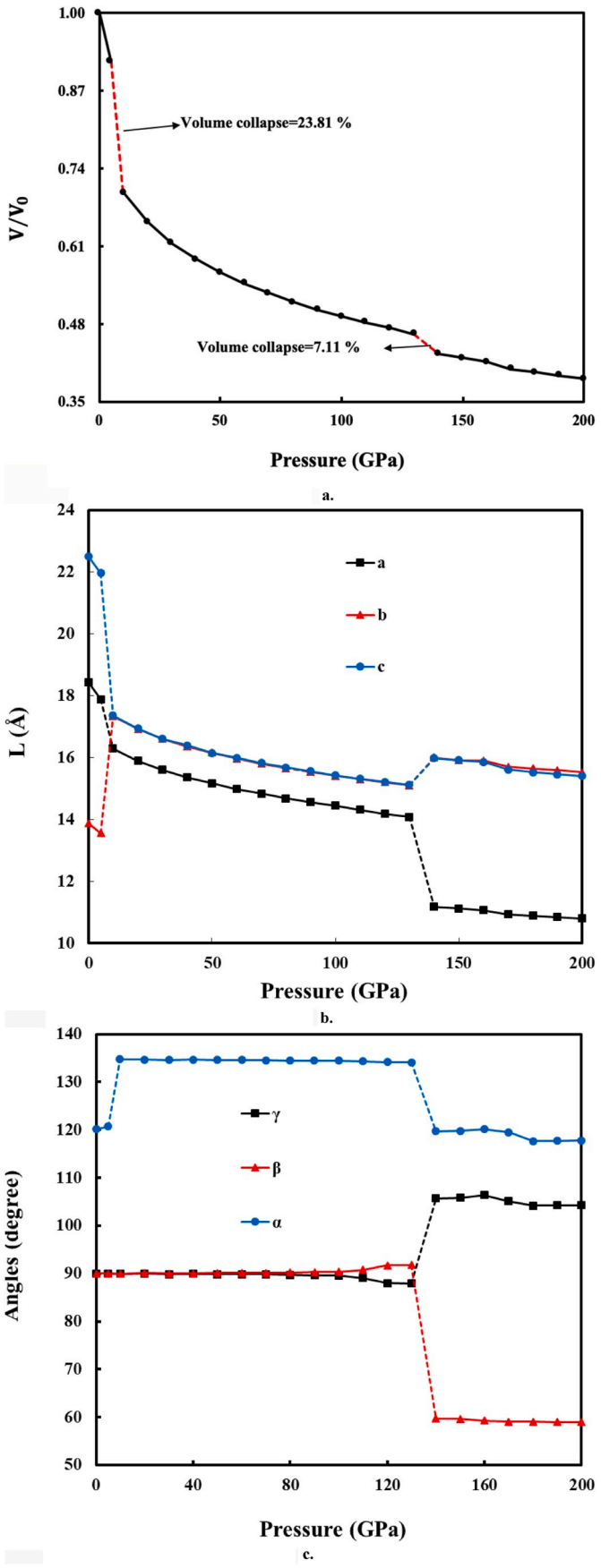

Fig. 2. The change in cell volume, lattice parameters and angle versus pressure.

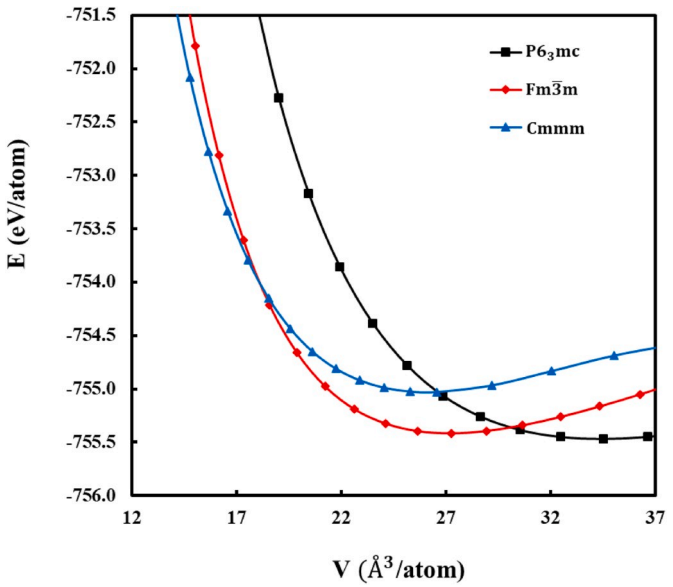

Fig. 3. The energy-volume change for phases of CdTe.

to apply increased pressure on the material, they achieved phase transition from this structure to NaCl type structure at 3.80 GPa. During the first transition, the volume collapse was 13.4% while it was 2.6% in the second transition. The low volume collapse in the second transition indicates that this cinnabar and NaCl structures are closely related. Starting from the NaCl type structure obtained, when the pressure value was reduced, cinnabar and zinc blende structures were obtained at 3.6 GPa and 2.7 GPa, respectively. This cinnabar structure obtained in both increase and decrease of the pressure value has a stable phase.

Therefore, it is worth noticing that the pressure-induced phase transformation mechanism of CdTe is very complex. In such a complex process of change, we decided to do this to clarify how pressure affects the wurtzite type structure of CdTe. We predicted phase transition sequence as $P6_3mc \rightarrow Fm\bar{3}m \rightarrow Cmmm$. We examined the structural, electronic, elastic, and vibration properties of all obtained structures. In addition, in order to get better information about the phase transition mechanism, the intermediate states was also examined in detail. Thus, it is believed that the results obtained will be guided to experimental workers.

2. Methods

In terms of density functional theory, some physical properties of CdTe such as structural, electronic, elastic, and phonon were studied with the Siesta program [8]. Perdew-Burke-Ernzerhof (PBE) function belonging to the generalized gradient approach (GGA) functional class was used for exchange-correlation energy [9]. Troullier-Martins type norm-conserving pseudopotentials for the Cd and Te atoms and double-zeta polarized (DZP) atomic orbital basis sets were preferred in calculations [10]. The mesh cut-off is energy that corresponds to the fineness of the real-space grid is sufficient to be 300 Rydberg (Ryd). For geometry optimizations, a higher value is sometimes needed. A higher value of the mesh cut-off gives a finer real-space grid and thus better accuracy. Using a periodic boundary condition with a 4 × 3 × 3 cell, a supercell of 144 atoms was modeled. The Brillouin zones (BZ) were sampled with a 7*x*7*x*4, 8*x*8*x*8 and 4*x*4*x*10 Monkhorst-Pack k-point mesh for $P6_3mc$, $Fm\bar{3}m$ and Cmmm phases, respectively [11]. Structural optimizations were applied to the system using the conjugate gradient (CG) technique. This process was continued until the residual force value acting on all atoms was smaller than 0.01 eV/A. Besides, the pressure was applied to the system in increments of 10 GPa using this CG technique. To analyze the structure at each applied pressure, the

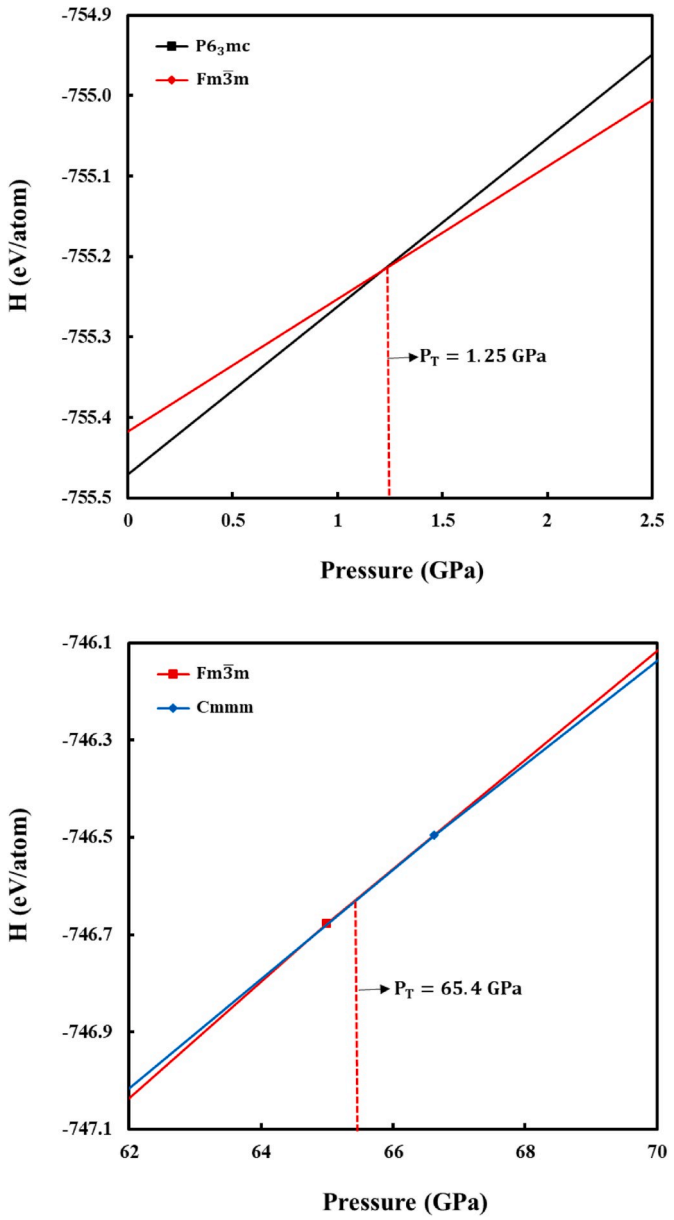

Fig. 4. The enthalpy variations of CdTe phases versus pressure.

minimization steps were investigated individually by using the KPlot program and RGS algorithm [12,13]. The purpose of this is to learn about lattice parameters, space groups and atomic coordinates at each pressure value applied to the material.

3. Results and discussions

The hexagonal type structure of CdTe corresponding to the $P6_3mc$ space group was studied under the pressure of 0 GPa. As a result of the structural optimizations, lattice parameters of this phase were obtained as a = b = 4.6006 Å and c = 7.5329 Å. CdTe in hexagonal structure has 4 atoms per unit cell. Cd and Te atoms are sites 2d (1/3, 2/3, 3/4) and 2c (1/3, 2/3, 1/4) Wyckoff positions, respectively. When the pressure of 10 GPa was applied to the hexagonal structure of CdTe, a cubic B1 structure corresponding to another stable structure space group $Fm\bar{3}m$ was observed. Lattice parameters were obtained as a = b = c = 6.0202 Å for B1. CdTe has 8 atoms per unit cell in this structure. Cd and Te atoms are sites 4a (0, 0, 0) and 4b (1/2, 1/2, 1/2) Wyckoff positions, respectively. When the gradually increasing pressure is applied to the B1 structure,

Table 1
The values of transition pressure, lattice parameters, volume, bulk modulus and derivate of bulk modulus for phases of CdTe.

Phases	P_t (GPa)	a (Å)	b (Å)	c (Å)	V (Å^3)	B_0 (GPa)	B_0'	References
P63mc*(#186)*	0	4.6006	4.6006	7.5329	159.43	49.90	4.53	This Study
		4.6740	4.6740	7.6640	167.42	35.50	5.20	[25]
		4.5499	4.5499	7.4512	154.25	45.4		[4]
Fm3¯m *(#225)*	1.25	6.0202	6.0202	6.0202	218.19	68.15	4.74	This Study
		6.1280	6.1280	6.1280	230.08	47.50	5.30	[25]
		5.7870	5.7870	5.7870	193.8	76.2	4.67	[26]
		6.1100	6.1100	6.1100		56.00	3.80	[27]
		5.9240	5.9240	5.9240		66.40	4.22	[28]
Cmmm*(#65)*	65.4	6.6198	6.4350	2.7938	119.01	67.65	4.46	This Study

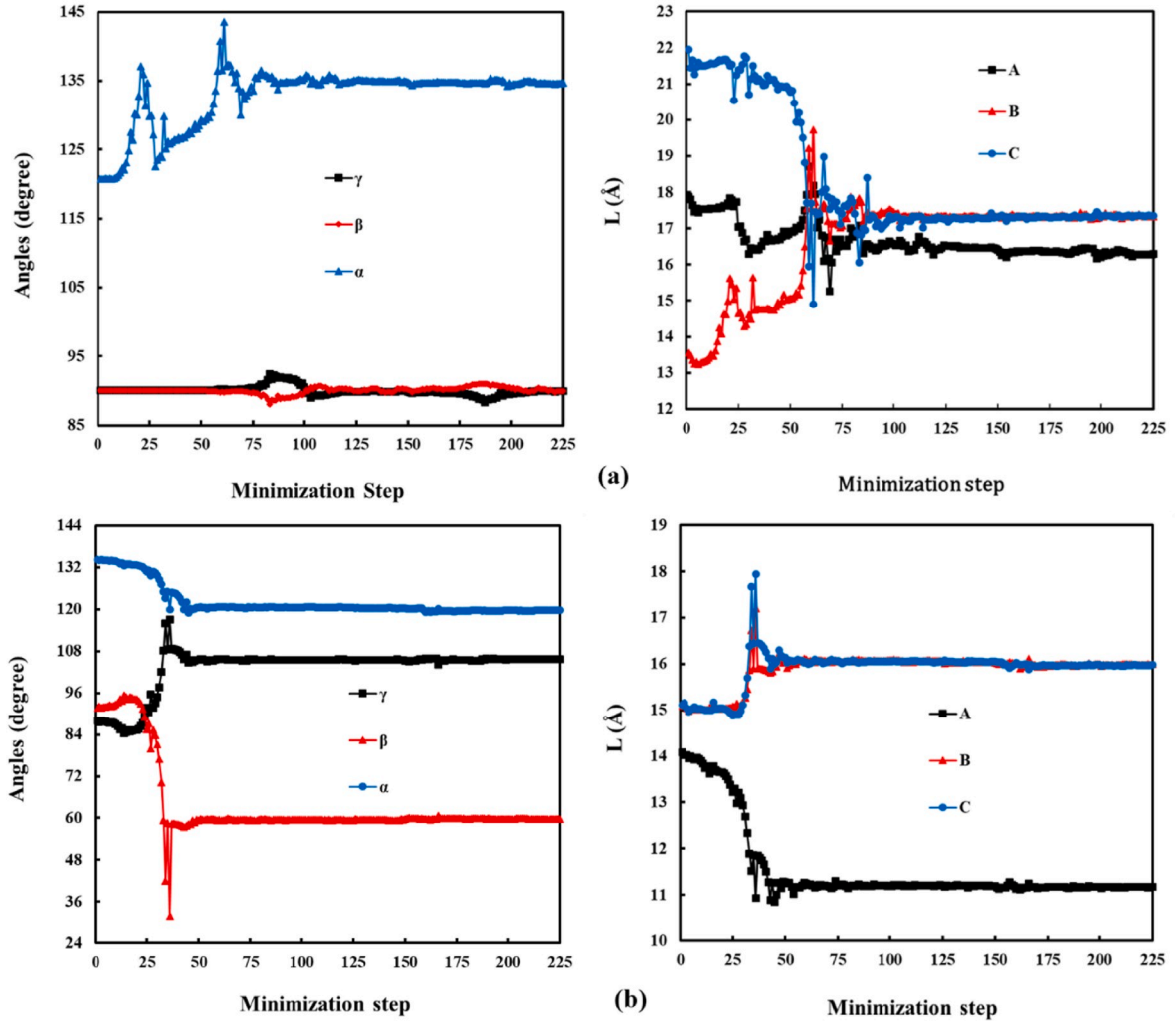

Fig. 5. Lattice vector lengths and the variation of the angles between these vectors for a) Fm$\bar{3}$m and b) Cmmm phases of CdTe.

we observed another stable structure at 140 GPa. This structure is an orthorhombic structure corresponding to the space group Cmmm. The lattice parameters of this structure are a = 6.6198, b = 6.4350 and c = 2.7938 Å. CdTe has 8 atoms per unit cell in this structure. Cd and Te atoms are sites 4j (0, y, 1/2) and 4 g (x, 0, 0) (x = 0.2702, y = 0.2232) Wyckoff positions, respectively. The images of these stable structures are shown in Fig. 1.

In order to investigate the phase transition under the applied hydrostatic pressure, the change of volume (V/V_0), angle and lattice parameters in the structure of supercell as a function of pressure were given in Fig. 2 a, b and c, respectively. As can be seen from Fig. 2, there is a sharp decrease in volume, lattice parameter and angle values at pressures of 10 GPa and 140 GPa. This sharp decrease shows us that the phase transition from one stable structure to another stable structure in CdTe is the first order.

All of these phases obtained under pressure are stable phases of CdTe. However, only one of them is the most stable phase. Therefore, in the next step, we have discussed the volume change as a function of energy in Fig. 3 to find out which phase is most stable for CdTe. As shown in Fig. 3, the $P6_3mc$ phase with the minimum energy is the most stable phase of CdTe. From Fig. 3 we can also predict the pressure value $(P = -dE_{tot}/dV)$ equal to the transition pressure (P_T) obtained from the enthalpy (H) calculation. The data obtained in the energy-volume calculations were fit to the third-order Birch-Murnaghan equation of state

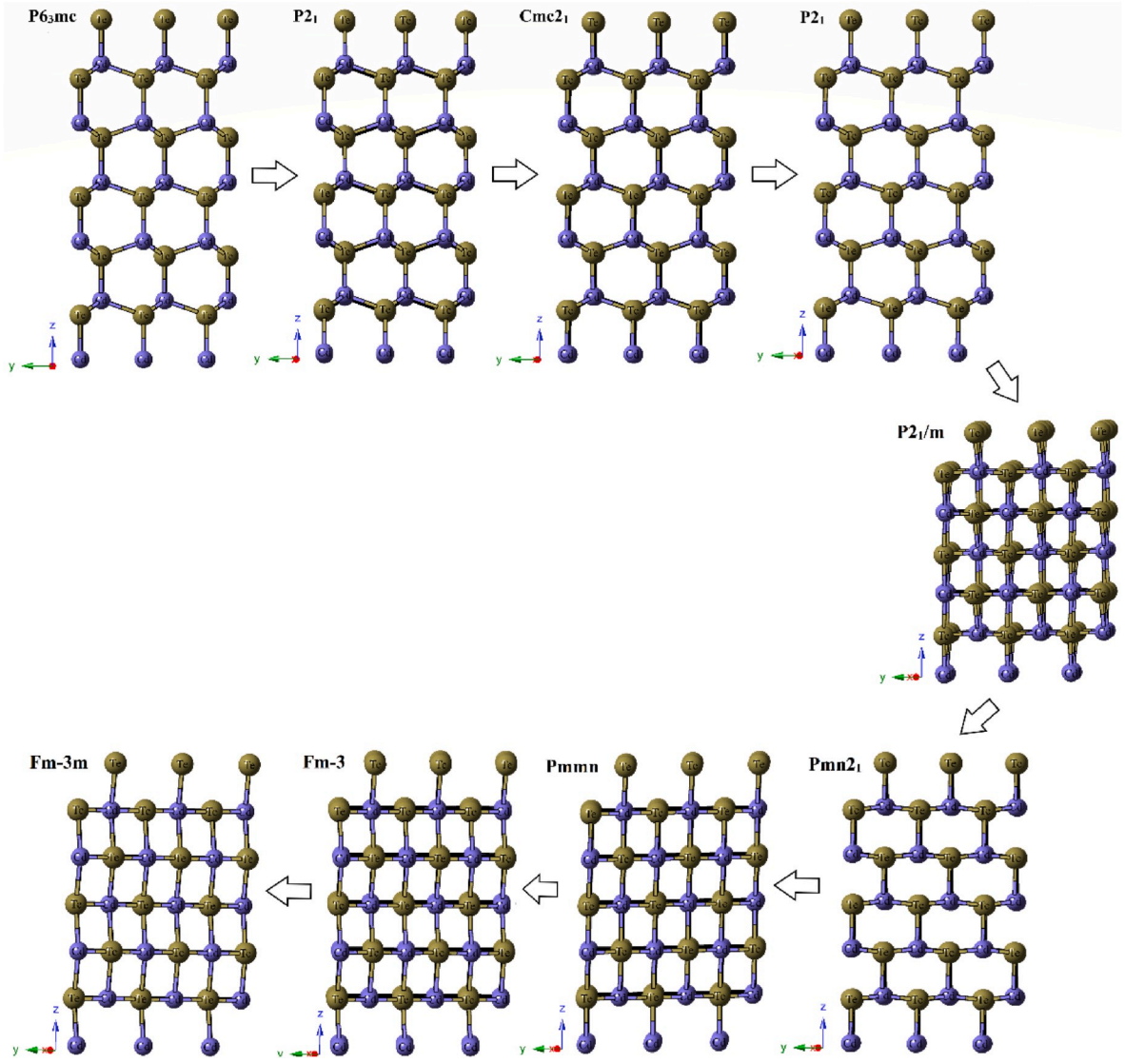

Fig. 6. Evolution of the Fm$\bar{3}$m structure.

Table 2
The space groups, lattice parameters, and angle values of intermediate states.

Phase	Minimization Steps	Space Groups	a (Å)	b (Å)	c (Å)	α	β	Γ
Fm$\bar{3}$m (#225)	15	$P2_1$ (#4)	4.3959	7.2241	4.0545	90.00	111.70	90.00
	31	$Cmc2_1$ (#36)	5.2172	6.3001	7.1701	90.00	90.00	90.00
	49	$P2_1$ (#4)	4.2287	6.9259	4.0258	90.00	105.06	90.00
	58	$P2_1/m$ (#11)	6.0458	5.3161	5.9816	90.00	98.06	90.00
	75	$Pmn2_1$ (#31)	4.0369	4.1272	5.8729	90.00	90.00	90.00
	81	Pmmn (#59)	5.6277	5.1270	4.2314	90.00	90.00	90.00
	111	Fm$\bar{3}$(#202)	5.8040	5.8040	5.8040	90.00	90.00	90.00
Cmmm (#65)	11	$R\bar{3}$m(#166)	3.4419	3.4419	3.4419	63.56	63.56	63.56
	35	P$\bar{1}$ (#2)	2.7333	3.0625	3.1770	114.48	96.91	111.31
	38	P4/mmm (#123)	3.1908	3.1908	2.9376	90.00	90.00	90.00

[14,15] given below.

$$E(V) = E_0 + \frac{9V_0B_0}{16}\left\{\left[\left(\frac{V_0}{V}\right)^{\frac{2}{3}} - 1\right]^3 B_0^{'} + \left[\left(\frac{V_0}{V}\right)^{\frac{2}{3}} - 1\right]^2 \times \left[6 - 4\left(\frac{V_0}{V}\right)^{\frac{2}{3}}\right]\right\} \quad (1)$$

where E(V) is the internal energy, E_0 and V_0 is energy and volume at zero pressure, respectively, V is the volume, B_0 is the bulk modulus and $B_0^{'}$ is the derivative of the bulk modulus with respect to pressure.

In this study, changes in the structure of CdTe were studied under hydrostatic pressure. Gradually increasing pressure such as 10, 20, 30 … 200 GPa was applied to the structure. The phase transition values obtained under hydrostatic pressure are generally higher than the

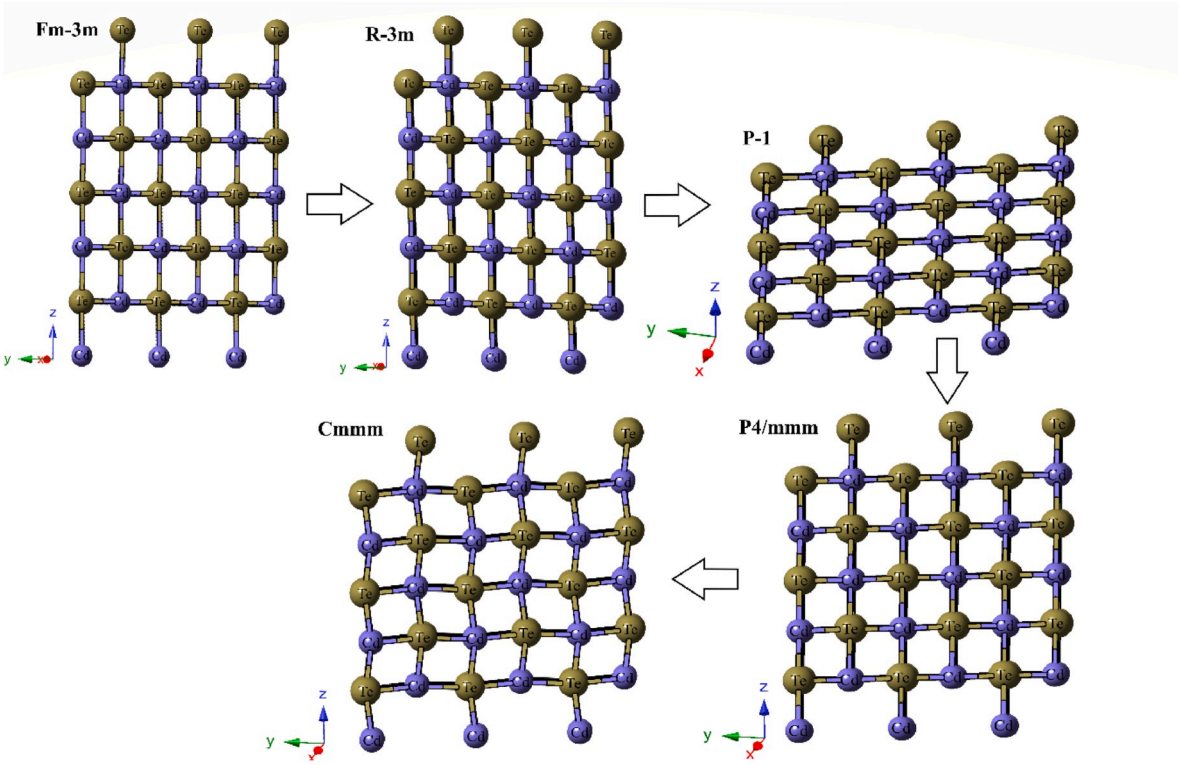

Fig. 7. Evolution of the Cmmm structure.

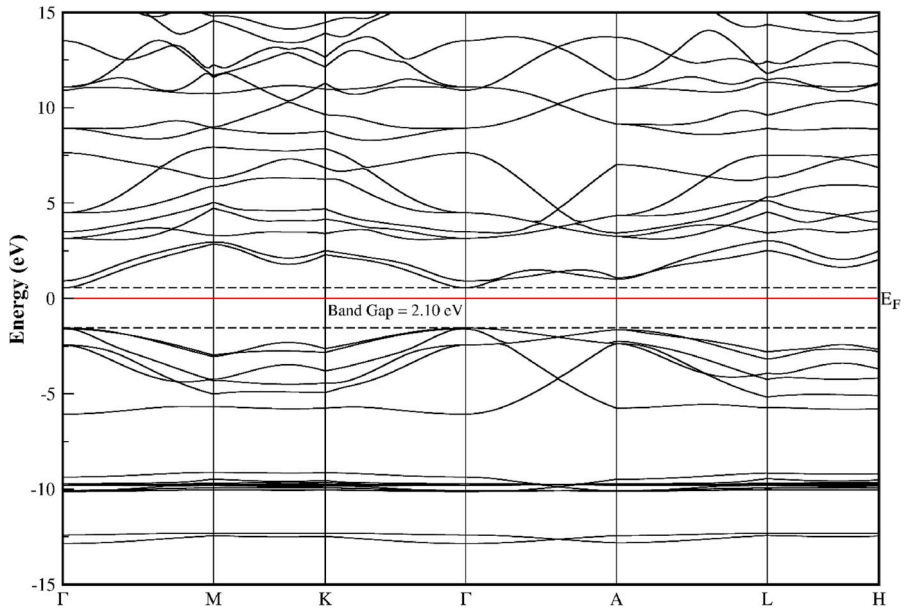

Fig. 8. Band structure for $P6_3mc$ phase of CdTe.

experimental results. The reason for obtaining this high transition pressure value is in fact due to some simulation conditions. In simulated systems, there are no surface effects and no defects due to periodic boundary conditions and the use of an ideal structured. In addition, another critical factor that may affect phase transformations is that the simulation time scale is very short compared to the experiment. In this short time, physical relaxation or reconstruction may not occur and thus may yield in frozen states in the simulations [16–19]. Contrariwise, the transition pressure value obtained from the enthalpy result is in good agreement with the experimental results. So in the next step, we consider the enthalpy calculation as a function of pressure in Fig. 4 using the thermodynamic equation ($G = H - TS$). G is Gibbs free energy and gives the transition pressure value in good agreement. Since the relaxation of the structure is carried out at zero Kelvin temperature, the term TS in Gibbs free energy is neglected so that G equals enthalpy given by eq. (2).

$$H = E_{tot} + PV \tag{2}$$

where, E_{tot}, P and V correspond to the total energy, pressure, and volume, respectively. As can be seen in Fig. 4, the point where the two

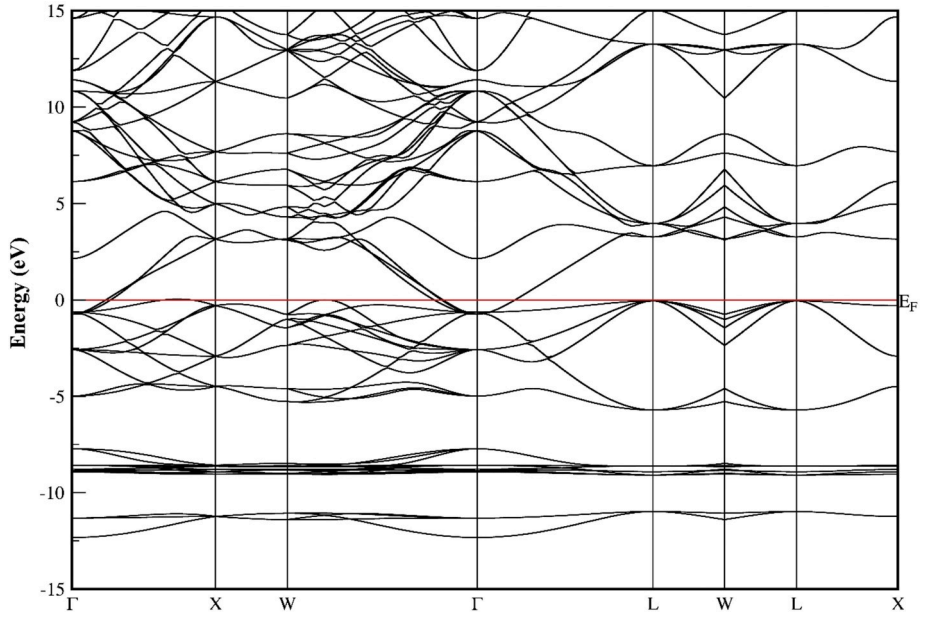

Fig. 9. Band structure for Fm$\bar{3}$m phase of CdTe.

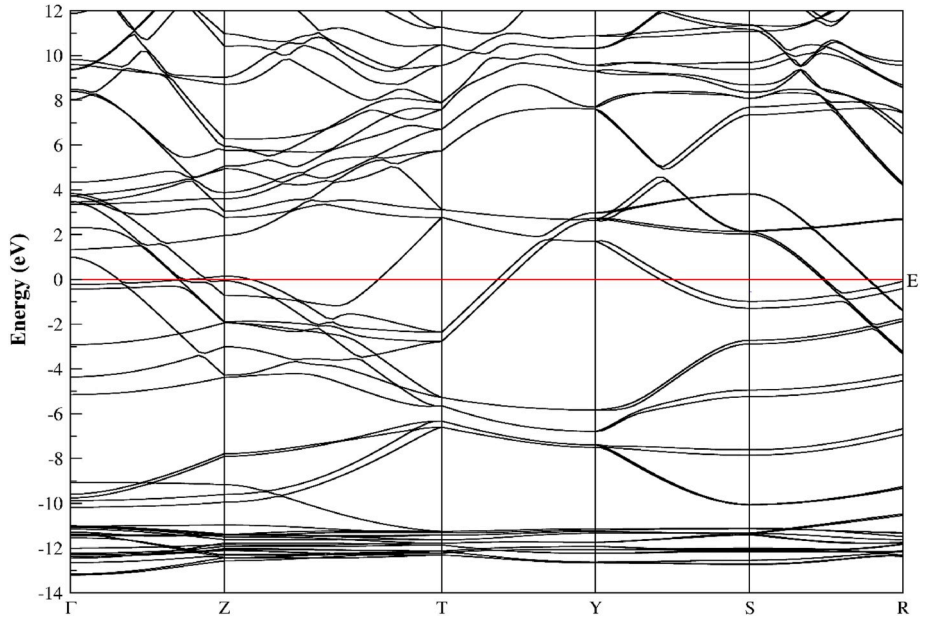

Fig. 10. Band structure for Cmmm phase of CdTe.

different phases intersect each other gives us the transition pressure value. We predicted the transition pressure values as 1.25 GPa for $P6_3mc \rightarrow Fm\bar{3}m$ and 65.4 GPa for $Fm\bar{3}m \rightarrow Cmmm$. In Table I, the values of transition pressure, lattice parameters, volume, bulk modulus and derivate of bulk modulus for all obtained phases of CdTe are given and compared with other studies in the literature.

We also investigated the lattice vector lengths (**A**, **B** and **C**) and the variation of the angles (γ, β, and α) between these lengths in each minimization step of the obtained structures at pressures of 10 GPa and 140 GPa. The lengths **A**, **B** and **C** correspond to [100], [010], and [001], respectively. γ, β, and α also correspond to angles between **A**, **B,** and **C** lengths. The change of these lengths and angles for each minimization step at 10 GPa and 140 GPa is given in Fig. 5 a and b, respectively.

As can be seen from the figure, the angle values of the hexagonal type structure of CdTe are $\alpha = \beta = 90^{\circ} and\ \gamma = 120^{\circ}$. γ and β angles did not change until the 75th minimization step, while the α angle increased to approximately 135°. Although there were small variations in γ and β angles after the 75th minimization step, they remained about 90° until the simulation was completed. The α angle did not change after the 75th minimization step and remained constant at about 135° until the end of the simulation. Until the 75th minimization step, the lengths A and C decreased and the length B increased to about 17 Ang. They then remained unchanged until the simulation was completed.

In Fig. 5b, the α, and β angles were reduced and the γ angle increased until the 30th minimization step. In this step, α is 120°, β is 60°, and γ is 108°. After this step, these values remained constant until the simulation was completed. In length variation, although the lengths B and C increased up to 50th minimization step, the length A decreased. In step 50, the lengths B and C are about 16 Å and length A is about 11 Å. After this step, A, B and C remained constant until the simulation was

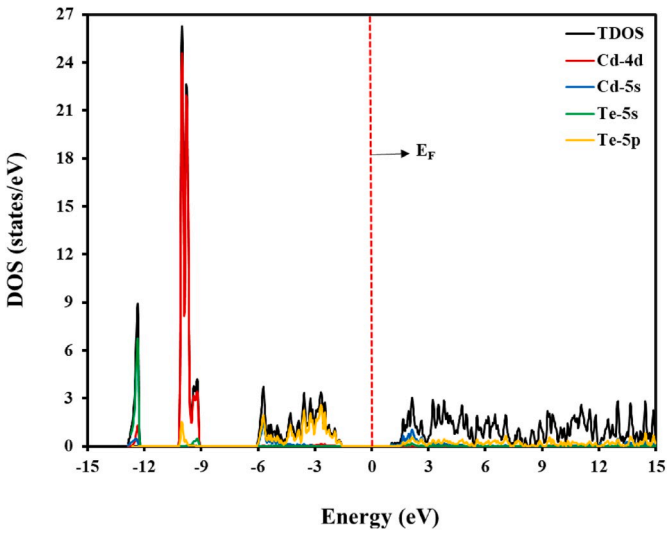

Fig. 11. The partial and total DOS for $P6_3mc$ phase of CdTe.

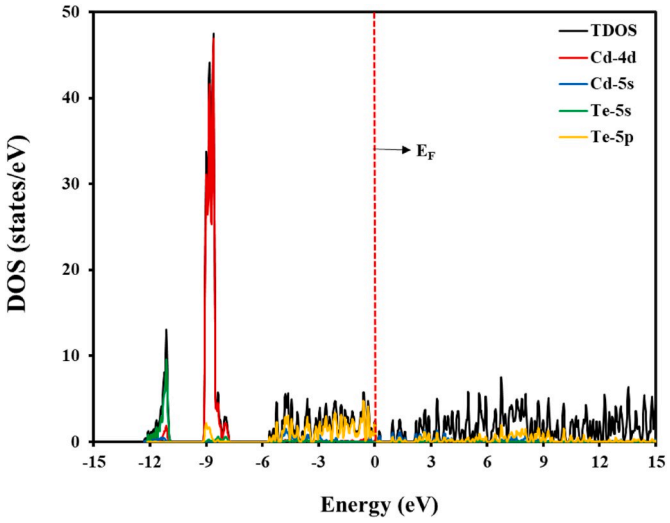

Fig. 12. The partial and total DOS for $Fm\bar{3}m$ phase of CdTe.

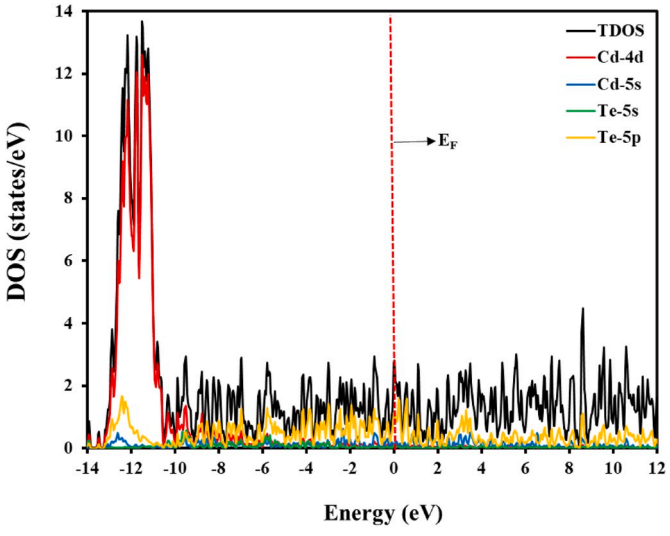

Fig. 13. The partial and total DOS for Cmmm phase of CdTe.

completed.

We tried to study the transition path of CdTe between the obtained high-pressure phases in detail. The minimization steps for the formation of the structures at 10 GPa and 140 GPa were analyzed individually with the KPlot program. In the first phase transition, the structure followed seven different paths from the $P6_3mc$ phase to the $Fm\bar{3}m$ phase, while in the second phase transition the structure followed three different paths from the $Fm\bar{3}m$ phase to the Cmmm phase. The formation of the structures obtained at 10 GPa and 140 GPa is given in Figs. 6 and 7 respectively. Some physical properties of these intermediate states such as space groups, lattice parameters, and angle values are given in Table II..

The electronic band structures calculated for the high-pressure phases of CdTe are given in (Figs. 8, 9 and 10). In all figures, the Fermi energy level was set to 0 and indicated by a red line. As shown in Figs. 8, 9 and 10, the $P6_3mc$ phase has a bandgap of 2.10 eV, while the $Fm\bar{3}m$ and Cmmm phases do not have a bandgap. This means that CdTe shows semiconductor properties in the $P6_3mc$ phase and metallic properties in $Fm\bar{3}m$ and Cmmm phases. In addition, the $P6_3mc$ phase of the CdTe is a semiconductor with direct band transition since both the valence and the conduction band are at the same point (Γ).

The calculated Density of States (total and partial) are given as a function of energy in for $P6_3mc$ (Fig. 11), $Fm\bar{3}m$ (Fig. 12), and Cmmm (Fig. 13) phases, respectively. The Fermi energy level was set to 0 and indicated by a red dotted line. From, the largest contribution below the fermi energy level for the $P6_3mc$ and $Fm\bar{3}m$ phase came from Te-5p between $(0)-(-9)$, Cd-4d between $(-9)-(-12)$ and Te-5s between $(-12)-(-15)$. For the Cmmm phase, the largest contribution came from Te-5p between $(0)-(-9)$ and Cd-4d between $(-9)-(-14)$ below the fermi energy level. Above Fermi energy, the largest contribution in all phases came from Te-5p (see Figs. 11, 12 and 13).

We also calculated the elastic constants to investigate the mechanical stability of the hexagonal structure which has five independent elastic constants ($C_{11}, C_{12}, C_{13}, C_{33}$, and C_{44}), the cubic structure which has three independent elastic constants (C_{11}, C_{12}, and C_{44}) and orthorhombic structure which has nine independent elastic constants ($C_{11}, C_{12}, C_{13}, C_{22}, C_{23}, C_{33}, C_{44}, C_{55}$, and C_{66}). Well-known Born criteria for the obtained structures of CdTe are defined as follows: $C_{44}>0, C_{11}>|C_{12}|, (C_{11}+2C_{12})C_{33}>2C_{13}^2$ for hexagonal structure [20, 21], $C_{11}>0, C_{44}>0, C_{11}>|C_{12}|, (C_{11}+2C_{12})>0$ for cubic structure [22,23], and $C_{11}>0; C_{11}C_{22}>C_{12}^2; C_{11}C_{22}C_{33}+2C_{12}C_{13}C_{23}-C_{11}C_{23}^2-C_{22}C_{13}^2-C_{33}C_{12}^2>0; C_{44}>0; C_{55}>0$, and $C_{66}>0$ for orthorhombic structure [24]. The calculated elastic constants are given in Table III. Looking at the data in Table III, the elastic constant C_{44} calculated for the orthorhombic structure is negative and all other calculated elastic constants are positive. When these elastic constants were fitted to the well-known Born criteria for the obtained structures, it was found that the hexagonal and cubic structures were mechanically stable and the orthorhombic structure was unstable.

In order to obtain information about the brittleness and ductility of the material, the bulk modulus (B) and shear modulus (G) for the high-pressure phases of CdTe were also calculated. If the B/G ratio is greater than 1.75, the material is ductile otherwise, the material is brittle. When we look at the data in Table III, the B/G ratio for all high-pressure phases of CdTe is greater than 1.75. Thus, the material is ductile in all phases.

In addition, the Poisson's ratio (ν) of the material at 0 GPa and high pressures were calculated. In the literature, the ν is 0.1 for covalent materials and 0.25 for ionic materials. The calculated ν for all phases of CdTe is greater than 0.25. Thus, the material is ionic in all phases. In order to investigate the elasticity of the material, we also calculated Young's modulus (E) which is the ratio of stress to strain. B, G, B/G, ν, and E values obtained for all phases of CdTe are given in Table III (see Table III).

Phonon dispersion curves for hexagonal and cubic structures of CdTe were calculated and given in Figs. 14 and 15, respectively. As can be

Table 3
Elastic constants (C_{ij} in GPa), shear modulus (G), bulk modulus (B), Young modulus (E), B/G ratio and Poisson's ratios (ν) for $P6_3mc$, $Fm\bar{3}m$ and Cmmm phases of CdTe.

Phases	C_{11}	C_{12}	C_{13}	C_{33}	C_{44}	C_{22}	C_{23}	C_{55}	C_{66}	G	B	E	B/G	ν
$P6_3mc$ (#186)	59.82	37.02	30.34	70.01	11.40	–	–	–	–	12.15	42.77	33.32	3.52	0.37
$Fm\bar{3}m$ (#225)	154.06	37.34	–	–	14.67	–	–	–	–	26.55	76.25	71.36	2.87	0.34
Cmmm (#65)	518.42	333.02	285.14	642.94	−497.76	460.53	312.69	125.62	126.49	72.54	384.96	204.77	5.30	0.41

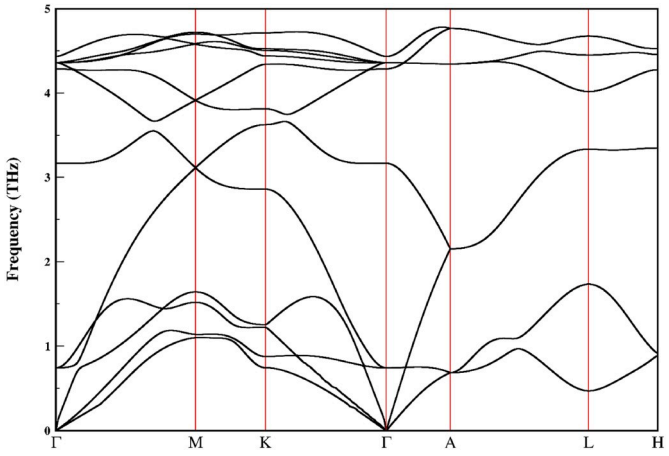

Fig. 14. The phonon dispersion curve for $P6_3mc$ phase of CdTe.

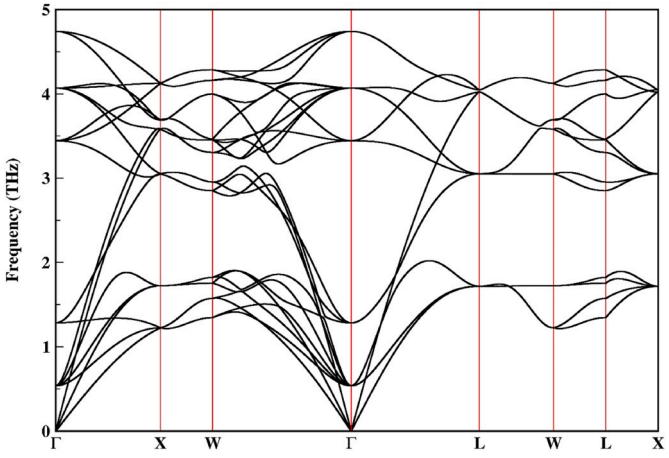

Fig. 15. The phonon dispersion curve for $Fm\bar{3}m$ phase of CdTe.

seen from the figures, CdTe does not have imaginary frequency branches in these two phases. Thus, CdTe is dynamically stable in these phases. However, the orthorhombic structure of CdTe was found to be mechanically unstable in the calculations of elastic constants. Since a mechanically unstable structure would also be dynamically unstable, we did not calculate a phonon for its orthorhombic structure..

4. Conclusions

The main purpose of this study is to investigate the $P6_3mc$ phase of CdTe under high pressure. $Fm\bar{3}m$ and Cmmm phases having two different crystal structures were obtained at 10 GPa and 140 GPa, respectively. The intermediate states which were meta-stable for these high-pressure phases were investigated in detail, which was first performed in this study. Electronic, elastic and phonon properties were also investigated for all predicted phases of CdTe. Although the $P6_3mc$ phase has a semiconductor property with a bandgap of 2.10 eV, the other two high-pressure phases are metallic because they do not have a bandgap. From the elastic constants and phonon calculations, it was seen that $P6_3mc$ and $Fm\bar{3}m$ phases were dynamically and mechanically stable and the Cmmm phase was unstable. In addition, B/G ratio and calculated v value were found to have ductile and ionic structure in all three phases.

References

[1] J. Mei, V. Lemos, Photoluminescence on CdSe and CdTe under hydrostatic pressure, Solid State Commun. 52 (1984) 785–788.
[2] M. Jain, II-VI Semiconductor Compounds, II-VI Semiconductor Compounds, in: JAIN MUKESH (Ed.), Published by World Sc ientific Publishing Co. Pte. Ltd., 1993. ISBN# 9789814439770.
[3] R.W. Birkmire, E. Eser, Polycrystalline thin film solar cells: present status and future potential, Annu. Rev. Mater. Sci. 27 (1997) 625–653.
[4] S.-H. Wei, S. Zhang, Structure stability and carrier localization in Cd X (X= S, S e, Te) semiconductors, Phys. Rev. B 62 (2000) 6944.
[5] R. Nelmes, M. McMahon, N. Wright, D. Allan, Phase transitions in CdTe to 28 GPa, Phys. Rev. B 51 (1995) 15723.
[6] H. Chun-Yuan, G. Chun-Xiao, L. Ming, H. Ai-Min, H. Xiao-Wei, Z. Dong-Mei, Y. Cui-Ling, W. Yue, Electron transport property of CdTe under high pressure and moderate temperature by in-situ resistivity measurement in diamond anvil cell, Chin. Phys. Lett. 24 (2007) 1070.
[7] M. McMahon, R. Nelmes, N. Wright, D. Allan, Phase transitions in CdTe to 5 GPa, Phys. Rev. B 48 (1993) 16246.
[8] P. Ordejón, E. Artacho, J.M. Soler, Self-consistent order-N density-functional calculations for very large systems, Phys. Rev. B 53 (1996). R10441.
[9] J.P. Perdew, K. Burke, M. Ernzerhof, Generalized gradient approximation made simple, Phys. Rev. Lett. 77 (1996) 3865.
[10] N. Troullier, J.L. Martins, Efficient pseudopotentials for plane-wave calculations, Phys. Rev. B 43 (1991) 1993.
[11] H.J. Monkhorst, J.D. Pack, Special points for Brillouin-zone integrations, Phys. Rev. B 13 (1976) 5188.
[12] R. Hundt, J.C. SchoÈn, A. Hannemann, M. Jansen, Determination of symmetries and idealized cell parameters for simulated structures, J. Appl. Crystallogr. 32 (1999) 413–416.
[13] A. Hannemann, R. Hundt, J. Schön, M. Jansen, A new algorithm for space-group determination,, J. Appl. Crystallogr. 31 (1998) 922–928.
[14] F. Birch, Finite elastic strain of cubic crystals, Phys. Rev. 71 (1947) 809.
[15] F. Murnaghan, The compressibility of media under extreme pressures, Proc. Natl. Acad. Sci. U.S.A. 30 (1944) 244.
[16] C. Kürkçü, A. Selgin, Z. Merdan, Ç. Yamçiçier, H. Öztürk, Investigation of structural and electronic properties of β-HgS: molecular dynamics simulations, Chin. J. Phys. 56 (2018) 783–792.
[17] C. Yamcicier, Z. Merdan, C. Kurkcu, Investigation of the structural and electronic properties of CdS under high pressure: an ab initio study, Can. J. Phys. 96 (2017) 216–224.
[18] H. Öztürk, M. Durandurdu, High-pressure phases of ZrO2: an ab initio constant-pressure study, Phys. Rev. B 79 (2009) 134111.
[19] S. Al, C. Kurkcu, C. Yamcicier, High pressure phase transitions and physical properties of Li2MgH4; implications for hydrogen storage, Int. J. Hydrogen Energy 45 (7) (2019) 4720–4730.
[20] A. Candan, S. Akbudak, Ş. Uğur, G. Uğur, Theoretical research on structural, electronic, mechanical, lattice dynamical and thermodynamic properties of layered ternary nitrides Ti2AN (A= Si, Ge and Sn), J. Alloys Compd. 771 (2019) 664–673.
[21] C. Kürkçü, Ç. Yamçıçıer, Structural, electronic, elastic and vibrational properties of two dimensional graphene-like BN under high pressure, Solid State Commun. 303 (2019) 113740.
[22] G. Surucu, A. Candan, A. Gencer, M. Isik, First-principle investigation for the hydrogen storage properties of NaXH3 (X= Mn, Fe, Co) perovskite type hydrides, Int. J. Hydrogen Energy 44 (2019) 30218–30225.
[23] G. Surucu, A. Candan, A. Erkisi, A. Gencer, H.H. Güllü, First principles study on the structural, electronic, mechanical and lattice dynamical properties of XRhSb (X= Ti and Zr) paramagnet half-Heusler antimonides, Mater. Res. Express 6 (2019) 106315.
[24] S. Akbudak, A. Candan, A. Kushwaha, A. Yadav, G. Uğur, Ş. Uğur, Structural, elastic, electronic and vibrational properties of XAl2O4 (X= Ca, Sr and Cd) semiconductors with orthorhombic structure, J. Alloys Compd. 809 (2019) 151773.
[25] S. Biering, The Unusual Structure of the Mercury Chalcogenides: Relativistic Effects in the Solid State, a thesis presented in partial fulfillment of the requirements for

the degree of Doctor of Philosophy at Massey University, Albany, New Zealand, in, Massey University, 2010.
[26] P. Van Camp, V. Van Doren, Structural phase transformation and ground state properties of cadmium telluride, Solid State Commun. 91 (1994) 607–610.
[27] S. Zerroug, F.A. Sahraoui, N. Bouarissa, Structural parameters and pressure coefficients for CdS x Te 1-x: FP-LAPW calculations, The European Physical Journal B 57 (2007) 9–14.
[28] N. Benkhettou, D. Rached, M. Rabah, Ab-initio calculation of stability and structural properties of cadmium chalcogenides CdS, CdSe, and CdTe under high pressure, Czech. J. Phys. 56 (2006) 409–418.